ACS APPLIED MATERIALS & INTERFACES

www.acsami.org

Research Article

Nonvolatile Electric Control of Rashba Spin Splitting in Sb/In_2Se_3 Heterostructure

Haixia Cheng, Xu Sun, Jun Zhou,* Shijie Wang, Hang Su,* and Wei Ji*

Cite This: https://doi.org/10.1021/acsami.4c07562

Read Online

ACCESS | Metrics & More | Article Recommendations | Supporting Information

ABSTRACT: Ferroelectric Rashba semiconductors (FRS) are highly demanded for their potential capability for nonvolatile electric control of electron spins. An ideal FRS is characterized by a combination of room temperature ferroelectricity and a strong Rashba effect, which has, however, been rarely reported. Herein, we designed a room-temperature FRS by vertically stacking a Sb monolayer on a room-temperature ferroelectric In_2Se_3 monolayer. Our first-principles calculations reveal that the Sb/In_2Se_3 heterostructure exhibits a clean Rashba splitting band near the Fermi level and a strong Rashba effect coupled to the ferroelectric order. Switching the electric polarization direction enhances the Rashba effect, and the flipping is feasible with a low energy barrier of 22 meV. This Rashba–ferroelectricity coupling effect is robust against changes of the heterostructure interfacial distance and external electric fields. Such a nonvolatile electrically tunable Rashba effect at room temperature enables potential applications in next-generation data storage and logic devices operated under small electrical currents.

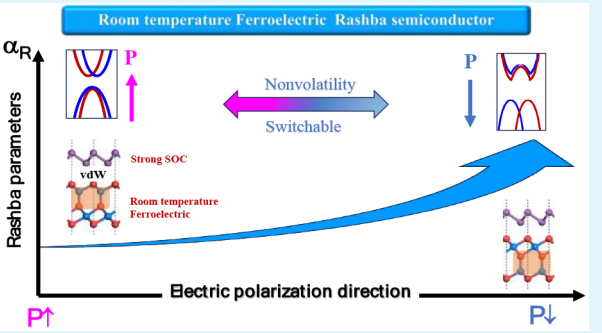

KEYWORDS: *ferroelectric Rashba semiconductor, heterostructure, two-dimensional materials, ferroelectricity, Rashba effect*

1. INTRODUCTION

Spintronics has attracted considerable attention for its potential in high-performance data storage and information transfer by manipulating the spin degree of freedom.[1−3] However, the utilization of ferromagnetic materials and the application of external magnetic fields for writing and reading spin states invariably result in an increase in both the device size and energy consumption, imposing constraints on their practical applications and hindering their further development.[4,5] Rashba spin−orbit coupling (SOC) offers a promising solution to these challenges, as it can facilitate the generation of spin-polarized electron states without a magnetic moment and enables control through a low-energy external electric field. In particular, ferroelectric Rashba semiconductors (FRS) combine the Rashba effect and ferroelectricity, allowing nonvolatile electrical control of spin current[6,7] via ferroelectric switching. Thus, it has superior scalability, lower power consumption, and the possibility for local manipulation of spin states.

Two-dimensional (2D) FRS have become particularly important as the miniaturization of spintronic devices.[8] Currently, a few 2D FRS have been reported, including $AgBiP_2X_6$ (X = S, Se, and Te),[9] $A_2P_2X_6$ (A = Al, Sc, Os, Ru, Sb, and Bi; X = S, Se, and Te), AB (A = Ge, Sn, Pb, Ga, In, Al, and Hg; B = O, S, Se, and Te)[8], distorted 1T-phase MX_2 monolayer[10], and 2H-phase MX_2 bilayers (M = Mo, W; X = S, Se, Te).[11] However, these FRS suffer from certain limitations, including small Rashba spin splitting, low operating temperature for ferroelectricity, and a lack of clean Rashba splitting bands, but with multiple band edges near the Fermi level. These constraints render them unsuitable for practical room-temperature applications. Recently, GeTe films have shown potential for room-temperature ferroelectricity, but their ferroelectric polarization switching efficiency is impacted by the Ge vacancy-induced conductivity in the material.[12] Therefore, discovering a novel FRS material with optimal properties remains paramount for advancing practical spintronics application.

The successful synthesis of 2D van der Waals (vdW) heterostructures[13,14] opens up an exciting avenue for the development of innovative hybrid materials/systems that integrate diverse functionalities. This prompts the exploration of whether a comparable strategy can be employed to achieve coupling between the ferroelectricity and the SOC effect. Of particular interest is the potential of this heterostructure to break inversion symmetry, induce the Rashba effect, and establish coupling between ferroelectricity and the Rashba

Received: May 8, 2024
Revised: August 8, 2024
Accepted: August 14, 2024

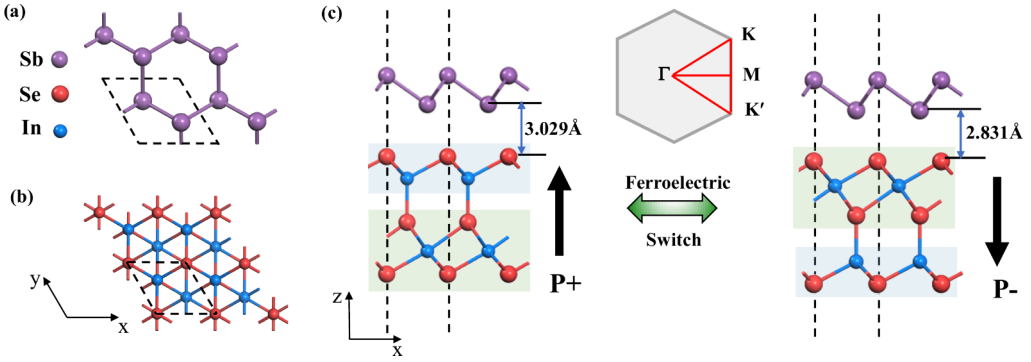

Figure 1. Top views of monolayer (a) Sb and (b) In_2Se_3. Side views of Sb/In_2Se_3 heterostructures with the In_2Se_3 ferroelectric dipole moment pointing (c) upward (left side) and downward (right side). Black rhombuses in (a) and (b) refer to the unit cells of monolayer Sb and In_2Se_3. The numerical values in (c) represent the interface distance between Sb and In_2Se_3. The inset in (c) is the 2D Brillouin zone. The black arrows in (c) represent the dipole moment direction in the In_2Se_3 layer.

effect. This paves the way for controllable modulation of the Rashba effect via switching the ferroelectric polarization direction.

In this work, we design an optimal ferroelectric Rashba semiconducting system by constructing a vertically stacked bilayer heterostructure between the easily exfoliable β-phase Sb semiconductor monolayer,[15] known for its strong SOC, with room-temperature ferroelectric α-phase In_2Se_3 monolayer.[16,17] Our density functional theory (DFT) calculations reveal that the heterostructure of Sb/In_2Se_3 induces Rashba splitting states, which can be tuned by the ferroelectric switching of the In_2Se_3 layer. Such strong coupling between Rashba and the ferroelectric state in the vdW heterostructure introduces a novel avenue for electronically controllable Rashba effects. It is noteworthy that several 2D magnet/In_2Se_3[18−20] and Sb/WTe_2[21] vdW heterostructures have been experimentally synthesized, underscoring the feasibility of the experimental realization of our proposed Sb/In_2Se_3 system.

2. METHODS

Density functional theory (DFT) calculations are performed using the projector augmented-wave[22,23] method, as implemented in the Vienna ab initio package.[24,25] The Perdew−Burke−Ernzerhof (PBE)[26] type generalized gradient approximation (GGA)[27] is used to treat the electron exchange-correlation interaction. The van der Waals (vdW) correction is applied using the optB86b-vdW method.[28−30] The energy cutoff for the plane wave basis is set to 500 eV. The Brillouin zone is sampled with Γ-centered 9 × 9 × 1 k mesh for structural relaxation and 13 × 13 × 1 for electronic structure analyses. Atomic positions and lattice constants are relaxed until the forces and energies are converged to 0.01 eV/Å for each atom and 10^{-6} eV/system, respectively. Spin−orbit coupling (SOC)[31] is incorporated in self-consistent energy and band structure calculations. Spin textures of Rashba states are obtained using the PyProcar open-source code.[32] Ferroelectric switching energy barrier is calculated by climbing image nudged elastic band (CI-NEB) method[33] with four intermediate images and a force convergence cutoff of 0.02 eV/Å. The initial and final states are the ferroelectric polarizations in upward and downward configurations, respectively.

The Sb/In_2Se_3 heterostructure is modeled using a 1 × 1 monolayers of Sb (Figure 1a) and α-In_2Se_3 (Figure 1b) with a good lattice mismatch of less than 0.24%. The calculated lattice parameters of 1 × 1 Sb and 1 × 1 α-In_2Se_3 monolayers are $a = b$ = 4.075 Å and $a = b$ = 4.074 Å, respectively, consistent with previous theoretical values,[16,34] indicating the validity of the calculation method and the adopted parameters. A vacuum space of about 20 Å is added along the c direction to avoid the interaction between adjacent layers for both the monolayer and Sb/In_2Se_3 heterostructure bilayer. The interface distance between Sb and In_2Se_3 layers is fully relaxed for all interface configurations. A dipole correction perpendicular to the heterostructure (along the c direction) is applied to eliminate spurious dipole−dipole interaction between periodic images and calculate the dipole moment.

3. RESULTS AND DISCUSSION

3.1. Structural Properties of Sb/In_2Se_3 Heterostructure. The Sb/In_2Se_3 heterostructure in a hexagonal lattice has two polarization configurations: (1) a P-up configuration, in which the middle-layer Se atoms are vertically aligned with the upper-layer In atoms (left panel of Figure 1c), resulting in an electric dipole pointing upward; (2) a P-down configuration, in which the middle-layer Se atoms are vertically aligned with the lower-layer In atoms (right panel of Figure 1c), resulting in an electric dipole pointing downward.

Three possible vertical stacking configurations including hollow, top, and bridge stackings are considered for the Sb/In_2Se_3 heterostructure as shown in Figure S1 of the Supporting Information. Among them, the hollow stacking (see Figure 1c), in which interfacial Sb atoms sit at the hollow sites of interfacial Se hexagons, is found to be energetically lower than the top (bridge) one by 113.627 (28.942) meV/unit cell and 140.864 (0.129) meV/unit cell for the P-up and P-down configuration, respectively. It is noted that the bridge stacking with downward polarization is unstable and relax to the hollow stacking after structure optimization. To examine the thermal stability of Sb/In_2Se_3 heterostructure, ab initio molecular dynamics (AIMD) simulations[35] are carried out in a canonical ensemble (NVT) using the algorithm of Nóse. The simulation is performed for a 3 × 3 × 1 supercell with a temperature of 500 K and a time step of 1.0 fs. The results (Figure S2) show that the variation of the free energy of Sb/In_2Se_3 heterostructure in both P-up and P-down are within ∼3 eV as well as the absence of bond breakage and large structure distortion in the final state, indicating their thermal stability at a high temperature. The phonon spectra are calculated by the PHONOPY code based on the density of functional perturbation theory using 3 × 3 × 1 supercells of the Sb/In_2Se_3 in both P-up and P-down configurations, respectively. As shown in Figure S3, there are only negligible imaginary modes around the Γ point,[36] confirming the dynamical stability of the Sb/In_2Se_3 heterostructure. Thus, Sb/In_2Se_3 refers to the hollow stacking configuration in the following, unless otherwise stated. The interface distance of the optimized Sb/In_2Se_3 heterostructure in the P-up configuration (3.029 Å) is

https://doi.org/10.1021/acsami.4c07562
ACS Appl. Mater. Interfaces XXXX, XXX, XXX−XXX

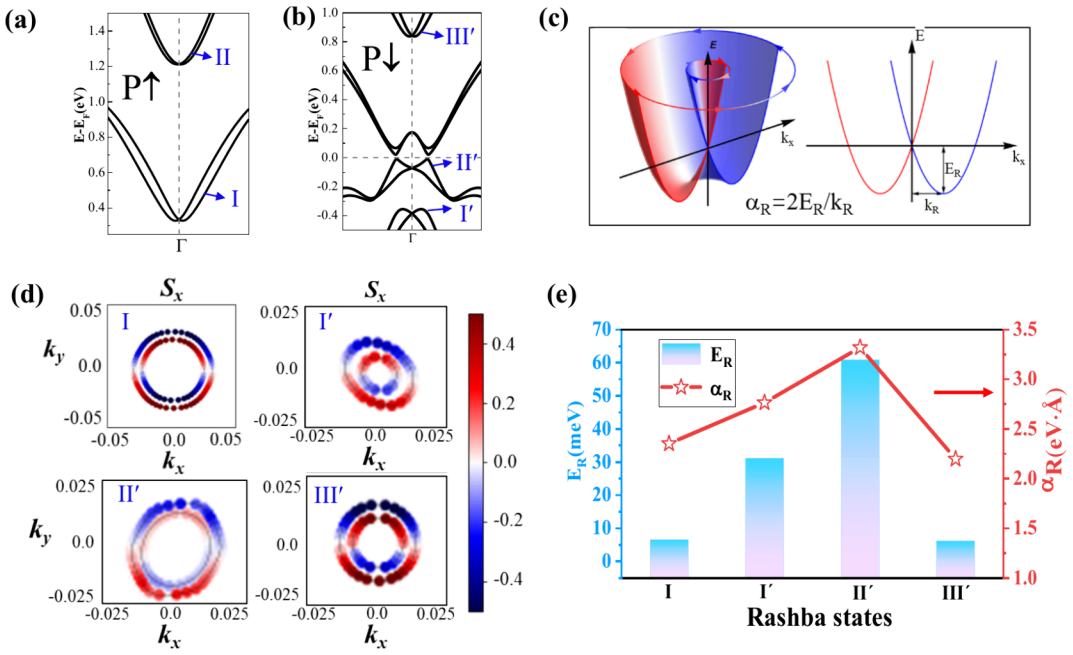

Figure 2. Calculated local band structures of Sb/In_2Se_3 heterostructures with SOC for (a) P-up and (b) P-down states. (c) Schematic of a band structure with Rashba-type spin splitting, where the spin is perpendicular to momentum k, E_R is the Rashba energy, k_R is the momentum shift, and α_R is the Rashba coupling parameter. The Fermi level is aligned to zero. (d) Spin textures with the S_x component of the Rashba state in P-up (state I) and in P-down (states I′, II′, and III′) configurations. The red and blue colors in color bar of (c) and (d) indicate the spin-up and spin-down components. (e) Calculated Rashba splitting gap and Rashba coupling parameter.

about 0.200 Å larger than that of the P-down configuration (2.831 Å). The interface binding energies are calculated using the equation

$$E_b = (E_{Sb} + E_{In_2Se_3} - E_H)/A$$

where E_b, E_{Sb}, $E_{In_2Se_3}$, E_H, and A refer to the total energy of the Sb layer, In_2Se_3 layer, heterostructure, and interface area, respectively. According to this equation, the positive interface binding energy represents an exothermic process for the formation of the Sb/In_2Se_3 heterostructure. The calculated interface binding energies of Sb/In_2Se_3 heterostructures are 0.493 and 0.601 J/m^2 (or 30.786 and 37.511 $meV/Å^2$) for P-up and P-down configurations, respectively. These results suggest a stronger interfacial interaction between Sb and In_2Se_3 for the P-down state. Besides, the interface binding energies of these vdW heterostructures are smaller than that of the traditional material interfaces and grain boundaries. For example, the interface binding energies for MgO/Co_2 and MgO/FeAl interfaces are 117 and 82 $meV/Å^2$, respectively,[37] while those for the ZrO_2 and HfO_2 grain boundaries are 1.18 and 1.36 J/m^2, respectively.[38]

3.2. Rashba−Ferroelectricity Coupling Effect of Sb/In_2Se_3 Heterostructure. The band structures of Sb/In_2Se_3 heterostructures in P-up and P-down configurations exhibit remarkable differences (see Figures S4a,b,d,e). In the P-up configuration, the band structure features a direct band gap of 0.731 eV at the Γ point without SOC, which reduces to 0.468 eV under SOC. Two types of Rashba-like spin splittings, labeled as states I and II, are observed in the conduction bands (Figure 2a), but no such splitting is present in the valence band. The typical characteristic of the Rashba effect is the appearance of momentum-dependent spin splitting in the absence of any external magnetic field or magnetic moment (see Figure 2c). The Rashba effect strength is decided by $\alpha_R = 2E_R/k_R$, where α_R is Rashba coupling parameter, E_R is the Rashba spin splitting gap, and k_R is momentum shift. The Rashba spin splitting gaps of states I and II are 6.640 and 1.080 meV, respectively. The small splitting gap of state II located at the high energy level makes it less practically useful for devices. Here, we mainly focus on state I. The energy contours with S_x spin component of state I at 0.70 eV above the Fermi level is displayed in Figure 2d. The spin textures between the outer and inner bands of the circular energy contours show opposite signs. Furthermore, the Rashba spin splitting primarily occurs in the in-plane (S_x, S_y) spin component rather than the out-of-plane component S_z (see Figure S4c), indicating the dominance of the Rashba spin−orbit interaction. The magnitude of the Rashba effect is 2.352 eV·Å for state I (see Figure 2e).

In contrast, when the ferroelectric polarization of In_2Se_3 points downward, the Sb/In_2Se_3 heterostructure changes from semiconducting in the P-up configuration to a gapless state without SOC (see Figures S4a,d). However, including SOC opens a small direct band gap of about 34 meV around the Fermi level and induces three Rashba-like states denoted as states I′, II′, and III′ (see Figure 2b). State II′ at the valence band maximum (VBM) displays a huge Rashba spin splitting gap of 60.860 meV, exhibiting a strong Rashba effect of 3.320 eV·Å, which is comparable to that of previously reported Rashba materials, such as BiAg alloy (3.7 eV·Å).[39] State I′ in the lower valence band and state III′ in the higher conduction band also exhibit prominent Rashba splitting gaps of 31.190 and 6.200 meV, respectively, with Rashba coupling parameters of 2.765 and 2.198 eV·Å, respectively (see Figure 2e). The energy contour of these states displays opposite signs between the outer and inner bands in spin texture (see Figure 2d), confirming the Rashba spin−orbital coupling effect. In other words, switching the ferroelectric polarization direction of

https://doi.org/10.1021/acsami.4c07562
ACS Appl. Mater. Interfaces XXXX, XXX, XXX−XXX

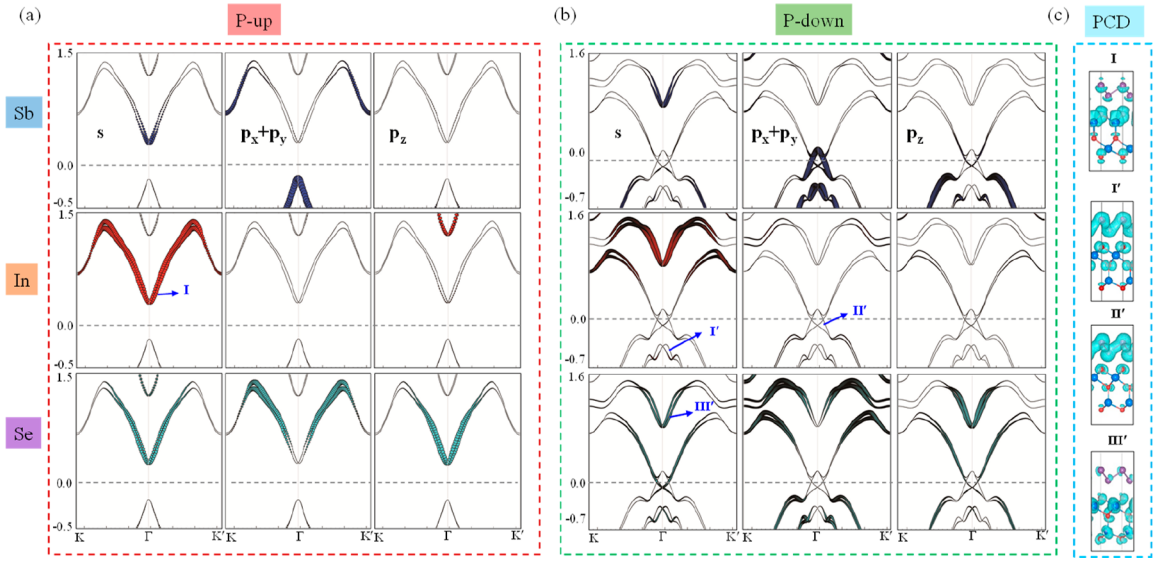

Figure 3. Orbital projected band structure with SOC of Sb/In_2Se_3 for (a) P-up and (b) P-down configurations. (c) Partial charge density (PCD) of the Rashba-like states I, I′, II′, and III′ at the Γ *k*-point of Sb/In_2Se_3 heterostructure. The isosurface value of PCD is 8×10^{-4} e/bohr^3.

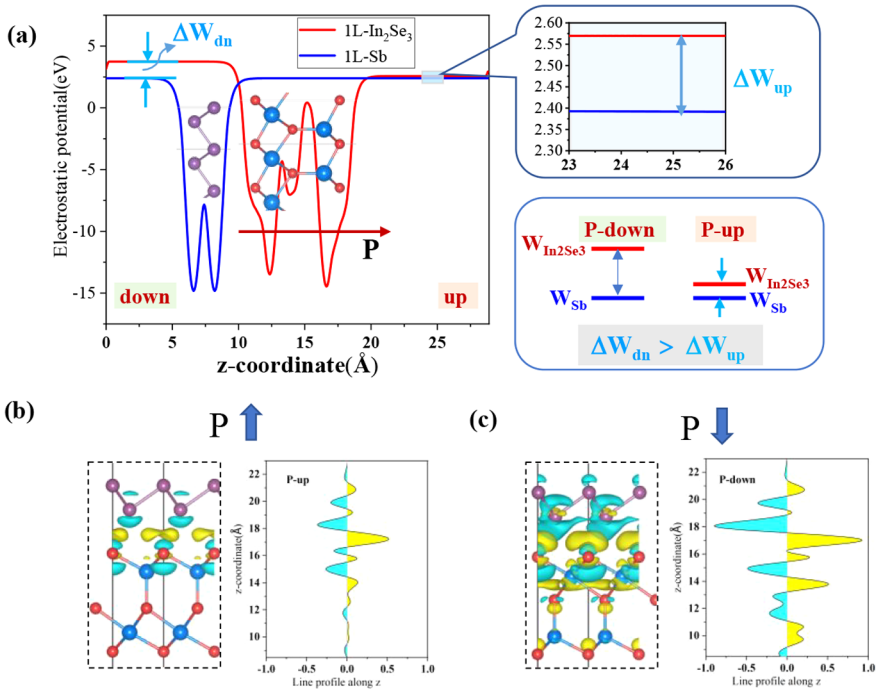

Figure 4. (a) Average electrostatic potential (EP) of monolayer Sb and monolayer In_2Se_3. Upper right is the enlarged electrostatic potential of monolayer Sb and In_2Se_3. Lower right is the schematic of work function difference between monolayer Sb and monolayer In_2Se_3 in P-up (ΔW_{up}) and P-down (ΔW_{dn}) Sb/In_2Se_3 heterostructure, respectively. (b, c) Differential charge density (DCD) in 3D view graph and line profile along the *z*-axis of Sb/In_2Se_3 heterostructure for P-up and P-down, respectively. The isosurface value of DCD is 2.5×10^{-4} e/bohr^3. The light yellow and light cyan isosurfaces in parts (b) and (c) refer to charge accumulation and reduction, respectively.

In_2Se_3 from up to down induces a stronger Rashba effect at the VBM for the Sb/In_2Se_3 heterostructure. This suggests a unique coupling between the Rashba effect and ferroelectric order in the Sb/In_2Se_3 heterostructures, which is not observed in pure monolayers Sb and In_2Se_3.

3.3. Mechanism of Ferroelectric Driven Rashba Effect.

To explore the origin of these Rashba states in the Sb/In_2Se_3 heterostructure for both the P-up and P-down configurations, we analyze their orbital projected band structures (Figures 3a,b) and partial charge density (PCD) (Figure 3c). The results show that state I is mainly contributed by the hybridization between the interfacial In-*s* and Se-*s*,p_z orbitals with a minor contribution from Sb-*s* of In_2Se_3 (Figures 3a,c). States I′ and II′ are mainly induced by the Sb-p_x and -p_y orbitals, with a minor contribution from the Sb-*s* and interfacial Se-*s* orbitals (Figures 3b,c). State III′ arises mostly from the In-*s*, Se-*s*,p_z, and Sb-*s* orbitals with small contributions from small Se-p_x,p_y orbitals of the In_2Se_3 layer (Figures 3b,c). Overall, states I, I′, and II′ demonstrate strong interfacial hybridization, while the interfacial hybridization for state III′ is not obvious

https://doi.org/10.1021/acsami.4c07562
ACS Appl. Mater. Interfaces XXXX, XXX, XXX−XXX

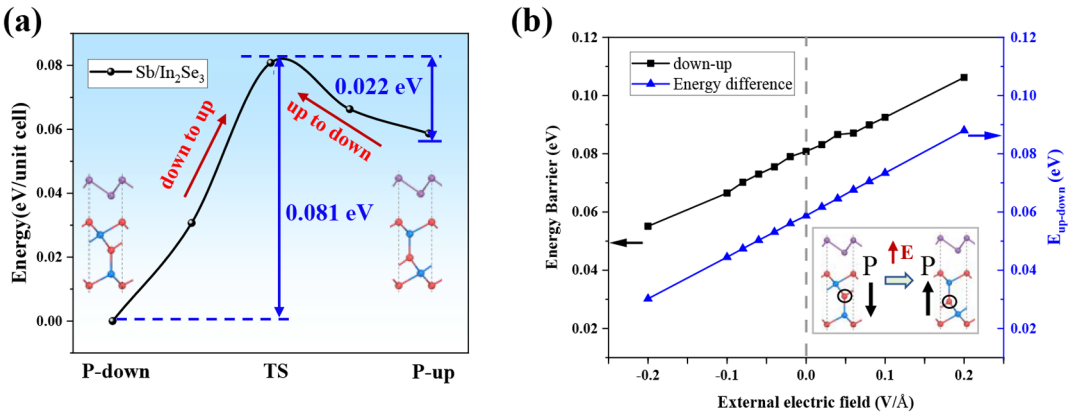

Figure 5. (a) Energy barrier of ferroelectric switching for Sb/In_2Se_3 heterostructure. Insets in (a) refer to the initial and final states structures of Sb/In_2Se_3. (b) Effect of an external electric field on the switching energy barrier from downward to upward and energy difference between P-up and P-down for Sb/In_2Se_3. Inset in (b) is a schematic for the ferroelectric polarization switch.

(see Figure 3c). And the mechanism behind Rashba states for the Sb/In_2Se_3 heterostructure changes from the interfacial $s-p_z$ orbital hybridization in the P-up configuration to the joint contribution of interfacial $s-p_x-p_y-p_z$ orbital hybridization in the P-down configuration. This is also confirmed by the orbital projected density of states for both the P-up and P-down heterostructures with SOC (Figure S5). The orbital projected band structures with SOC of monolayer Sb, monolayer In_2Se_3, and Sb/In_2Se_3 heterostructure are also given in Figure S6 for a direct comparison, which clearly shows that the Rashba states are driven by the interface interaction.

The significant difference in band structures of the Sb/In_2Se_3 heterostructure caused by reversing ferroelectric polarization of In_2Se_3 could be explained by two factors: the difference in work function between the Sb and In_2Se_3 layers (see Figure 4a) and the differential charge density (DCD) within the Sb/In_2Se_3 heterostructure (see Figures 4b,c). The Sb monolayer is symmetric with an identical electrostatic potential on both sides (blue line in Figure 4a). Conversely, the In_2Se_3 monolayer exhibits broken mirror symmetry, resulting in a difference in electrostatic potential along its two sides (denoted as up and down side, indicated by the red line in Figure 4a). The calculated work function for the Sb monolayer is 4.701 eV, while for the In_2Se_3 monolayer it is 5.673 eV for the up side and 6.486 eV for the down side. When the Sb monolayer contacts the opposite-polarized In_2Se_3 monolayer, the work function difference between Sb and In_2Se_3 in the P-up state (ΔW_{up}) is 0.972 eV, which is lower than that of the P-down state (ΔW_{dn} = 1.785 eV). The difference of the ΔW_{up} and ΔW_{dn} corresponds to the effective potential offset between up and down side of the monolayer In_2Se_3, reflecting the band gap offset observed in Figure S4. As a result, fewer electrons are transferred from Sb to In_2Se_3 for P-up Sb/In_2Se_3 (see Figure 4b), maintaining a larger Sb−Se interface distance. In contrast, there is noticeable electron transfer between Sb and In_2Se_3 in the P-down Sb/In_2Se_3 heterostructure due to their significant work function difference (Figure 4c), leading to a smaller Sb−Se interface distance compared to that of P-up Sb/In_2Se_3. It is interesting to note that similar mechanisms have been proposed for the adsorption of metal porphyrazine molecules or gas molecules on the surface of the In_2Se_3 monolayer.[40,41] The modulated charge distribution around the interface contributes to the variation in the electronic band structure of Sb/In_2Se_3 between the P-up and P-down states.

3.4. Ferroelectric Properties of Sb/In_2Se_3 Heterostructure. As discussed above, the different band alignments of Sb and In_2Se_3 between the P-up and P-down configurations lead to different overall ferroelectric polarization strength. The total dipole moments for the P-up and P-down configuration are 0.102 and 0.047 e·Å, respectively. Compared to the pure In_2Se_3 monolayer (0.091 e·Å), the dipole moment is enhanced in the P-up configuration and is reduced in the P-down configuration. To explain this, we calculated the average electrostatic potentials (EP) of the Sb/In_2Se_3 heterostructure for both polarization states, which reveals the existence of two dipole moments: an intrinsic dipole moment in In_2Se_3 ($D_{In_2Se_3}$) and a Sb−Se interfacial dipole moment (D_{inter}) (see Figures S7a,b). $D_{In_2Se_3}$ remains dominant with a value of ∼0.091 e·Å between different polarization states, while D_{inter} is ∼0.011 and 0.044 e·Å for the P-up and P-down configuration, respectively. These differences in the interfacial dipole moment among different polarized heterostructure also impact the band structure and interface distance.

Switching the electric polarization direction in ferroelectric materials is crucial for practical applications. We employ the climbing image nudged elastic band method to investigate the feasibility of ferroelectric switching. In Figure 5a, the P-down Sb/In_2Se_3 has a lower energy than the P-up state by 59 meV/f.u. The energy barrier for the ferroelectric switching from up to down and the opposite is 22 and 81 meV, respectively. These values are smaller than those in experimentally realized ferroelectric materials such as $CuCrP_2S_6$ (100 meV/f.u.). The calculated ferroelectric energy barrier for monolayer In_2Se_3 is 23 meV (Figure S8), consistent with another calculation,[16] indicating that the electric polarization direction in the Sb/In_2Se_3 heterostructure can be easily switched from up to down, similar to that of monolayer In_2Se_3. However, switching from down to up requires a relatively higher external electric field.

To assess the feasibility of reversing the polarization direction of the Sb/In_2Se_3 heterostructure using an external electric field, we study the impact of field strengths ranging from −0.2 to 0.2 V/Å along the z direction on the energy barrier for ferroelectric switching (Figure 5b). We focus on the effect of external electric field on the energy barrier from downward to upward since it has a higher energy barrier than the reverse process. The energy barrier for switching from

https://doi.org/10.1021/acsami.4c07562
ACS Appl. Mater. Interfaces XXXX, XXX, XXX−XXX

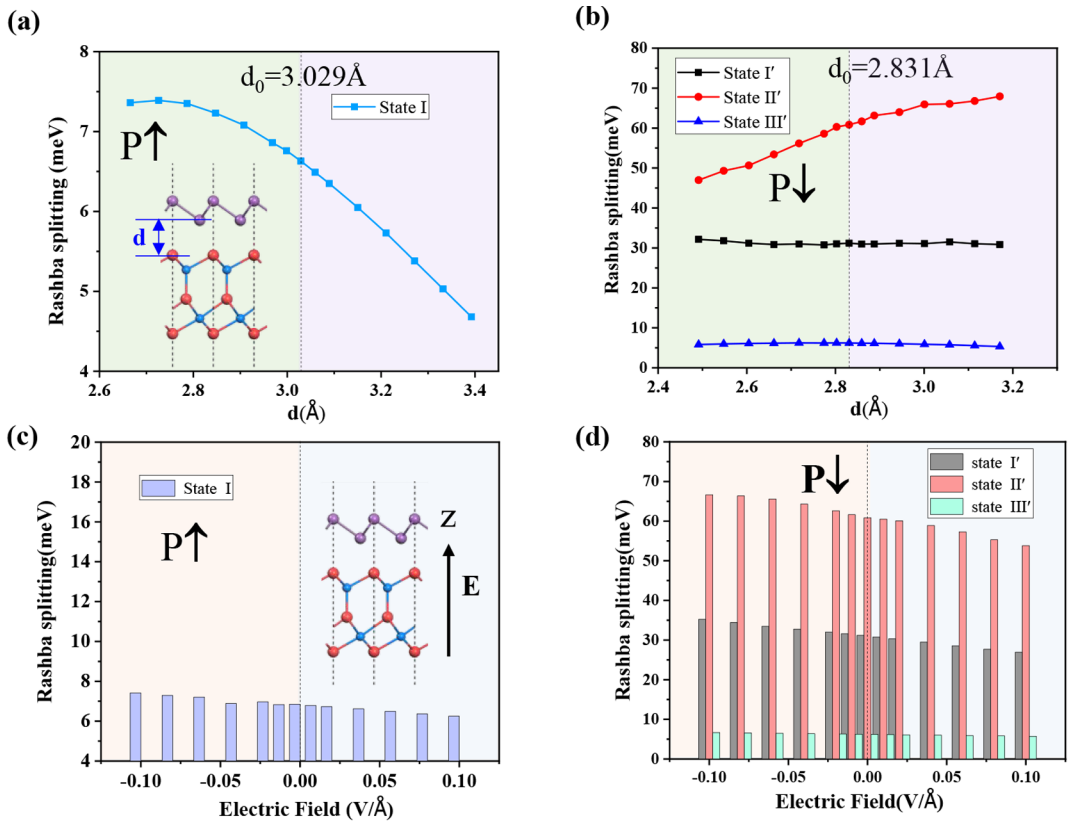

Figure 6. Evolution of Rashba splitting gap of Sb/In_2Se_3 with (a, c) P-up and (b, d) P-down of In_2Se_3 under various Sb−Se vertical interface distances and external electric fields. The vertical dashed lines in (a) and (b) refer to the equilibrium interfacial spacing position d_0.

downward to upward increases to 115 meV at 0.2 V/Å and decreases to 55 meV at −0.20 V/Å. This is because that the interface dipole moment D_{inter} (point upward) is antiparallel to the intrinsic $D_{In_2Se_3}$ (point downward) (see Figure S7b). Thus, applying a negative external electric field to Sb/In_2Se_3 initially offsets the interface electric field D_{inter}, making it closer to the value in pure monolayer In_2Se_3, resulting in a lower switch energy barrier. The evolution of dipole moments of P-down Sb/In_2Se_3 with an out-of-plane external electric field also confirms this conclusion (see Figure S9). It is noted that the largest external electric field applied in this study exceeds the typical values used for practical devices. For instance, the coercive field for ferroelectric materials like HfO_2 is around 0.02 eV/Å.[42] The larger value used here is to facilitate a more pronounced energy barrier or energy difference between the up and down configurations under the external electric field.

We also investigate the stability of the Sb/In_2Se_3 heterostructure with opposite polarization under an external electric field. As shown in Figure 5b, the P-down state is always more stable than the P-up state regardless of whether a positive or negative electric field is applied. Moreover, with the increase of the negative electric field, the energy difference between the two states decreases gradually, demonstrating that a negative electric field could promote to form a ferroelectric bistable state. Therefore, the application of an external electric field can significantly facilitate the ferroelectric polarization switch.

3.5. Effects of Different Interface Distances and External Electric Field on the Rashba Effect. The discussion in Section 3.3 highlights the tunable Rashba effect of Sb/In_2Se_3 by the polarization state of In_2Se_3, which also alters the interfacial distance between the Sb and In_2Se_3 layer. Herein, we examine the impact of varying the vertical interface distance (denoted as d) between Sb and In_2Se_3 on the Rashba effect in both P-up and P-down configurations. The interlayer distance is changed by rigidly shifting the Sb layer, while keeping the In_2Se_3 layer fixed. As shown in Figure 6a, the reduction of the interfacial distance from the initial value d_0 = 3.029 Å to d = 2.665 Å (shrink by 12%) slightly increases the Rashba spin splitting gap of state I at the conduction band minimum (CBM) in the P-up configuration. Conversely, the increase in the distance to 3.392 Å reduces the Rashba spin splitting gap by 2 meV. This behavior can be attributed to the hybridization of interfacial Sb and In_2Se_3 layers, which contributes to state I and is dependent on the interface vertical distance. In the P-down configuration (Figure 6b), state I′ in the lower valence band and state III′ in the higher conduction band exhibit negligible sensitivity to changes in interface distance. The splitting gap of state II′ in VBM decreases by about 13.86 meV as the distance decreases from 2.831 to 2.491 Å (shrink by 12%) and slightly increases with the interface distance increases. Thus, the Rashba splitting at VBM of P-down configuration is relatively sensitive to changes in the interface distance due to its stronger interface hybridization interaction compared to the P-up configuration. The Rashba coupling parameter exhibits a small variation of less than 1 eV·Å for a range of interface distance changes within ±12%, as depicted in Figure S10a. In general, the interface distance has little effect on the Rashba effect of the Sb/In_2Se_3 heterostructure.

The effect of an external out-of-plane electric field, ranging from −0.1 to −0.1 V/Å along the z direction, on the Rashba effect for both of P-up and P-down Sb/In_2Se_3 heterostructure

https://doi.org/10.1021/acsami.4c07562
ACS Appl. Mater. Interfaces XXXX, XXX, XXX−XXX

is also studied. As shown in Figure 6c, the external electric field has minimal effect on P-up's Rashba spin splitting, changing by only about 1 meV under ±0.1 V/Å. The influences for the Rashba spin splitting of states I′ and II′ in the P-down configuration are also not significant (Figure 6d). State III′, similar to state I, remains robust against the external electric field. The external electric field within the scale of ±0.1 V/Å also has a slight effect on the Rashba coupling parameters of Sb/In_2Se_3 for both P-up and P-down, as shown in Figure S10b. These results suggest that spin precession can be effectively tuned with a gate voltage.[43]

4. CONCLUSIONS

In this work, we systematically investigate geometric and electronic properties of the Sb/In_2Se_3 heterostructures in opposite polarization directions using first-principles calculations. Our results show that the P-down configuration exhibits stronger interface binding strength than the P-up one. Both P-up and P-down Sb/In_2Se_3 heterostructures show a strong Rashba effect driven by the SOC effect and the broken inversion symmetry. Switching the ferroelectric polarization from up to down results in a change of the Rashba states from the CBM to the VBM, enhancing the Rashba effect. A small external electric field could effectively flip the ferroelectric polarization direction from up to down due to its lower energy barrier. The Rashba−ferroelectric coupling effect remains robust against changes in interface distance and external electric field. This work opens up a new pathway to obtain 2D FRS through regulating interlayer coupling and fine-tuning electronic band structure by forming a 2D van der Waals heterostructure.

■ ASSOCIATED CONTENT

Supporting Information

The Supporting Information is available free of charge at https://pubs.acs.org/doi/10.1021/acsami.4c07562.

Structures of the Sb/In_2Se_3 heterostructure with different stacking types; AIMD simulation for P-up and P-down Sb/In_2Se_3 at 500 K; phonon dispersion spectrum, band structures, spin texture, PDOS and averaged electrostatic potential of Sb/In_2Se_3 heterostructures for P-up and P-down; orbital projected band structures of ML Sb, ML In_2Se_3 and Sb/In_2Se_3 heterostructure; ferroelectric switching energy barrier for monolayer In_2Se_3; dipole moments of P-down Sb/In_2Se_3 under various out-of-plane electric field; Rashba coupling parameter of both P-up and P-down Sb/In_2Se_3 under various interface distances and out-of-plane external electric fields (PDF)

■ AUTHOR INFORMATION

Corresponding Authors

Jun Zhou − *Institute of Materials Research and Engineering (IMRE), Agency for Science, Technology and Research (A*STAR), Singapore 138634, Republic of Singapore;* orcid.org/0000-0002-5505-7616; Email: zhou_jun@imre.a-star.edu.sg

Hang Su − *Material Digital R&D Center, China Iron & Steel Research Institute Group, Beijing 100081, China;* Email: hangsu@vip.sina.com

Wei Ji − *Beijing Key Laboratory of Optoelectronic Functional Materials & Micro-Nano Devices, Department of Physics, Renmin University of China, Beijing 100872, China; Key Laboratory of Quantum State Construction and Manipulation (Ministry of Education), Renmin University of China, Beijing 100872, China;* orcid.org/0000-0001-5249-6624; Email: wji@ruc.edu.cn

Authors

Haixia Cheng − *Material Digital R&D Center, China Iron & Steel Research Institute Group, Beijing 100081, China*

Xu Sun − *Material Digital R&D Center, China Iron & Steel Research Institute Group, Beijing 100081, China; Division of Functional Materials, Central Iron and Steel Research Institute, Beijing 100081, China*

Shijie Wang − *Institute of Materials Research and Engineering (IMRE), Agency for Science, Technology and Research (A*STAR), Singapore 138634, Republic of Singapore;* orcid.org/0000-0001-6312-3524

Complete contact information is available at: https://pubs.acs.org/10.1021/acsami.4c07562

Notes

The authors declare no competing financial interest.

■ ACKNOWLEDGMENTS

This research was supported by the National Key Research Project (Grant No. 2021YFB3501502, 2022YFB3505202, and 2021YFB3701201) of the Ministry of Science and Technology of China, National Natural Science Foundation of China (Grant No. 11974422), Strategic Priority Research Program of the Chinese Academy of Sciences (Grant No. XDB30000000), Fundamental Research Funds for the Central Universities, and Research Funds of Renmin University of China (Grant No. 22XNKJ30).

■ REFERENCES

(1) Lin, X.; Yang, W.; Wang, K. L.; Zhao, W. Two-dimensional Spintronics for Low-power Electronics. *Nat. Electron.* **2019**, *2* (7), 274−283.

(2) Žutić, I.; Fabian, J.; Das Sarma, S. Spintronics: Fundamentals and Applications. *Rev. Mod. Phys.* **2004**, *76* (2), 323−410.

(3) Jansen, R. Silicon Spintronics. *Nat. Mater.* **2012**, *11* (5), 400−408.

(4) Allwood, D. A.; Xiong, G.; Faulkner, C. C.; Atkinson, D.; Petit, D.; Cowburn, R. P. Magnetic Domain-wall Logic. *Science* **2005**, *309* (5741), 1688−1692.

(5) Awschalom, D. D.; Flatté, M. E. Challenges for Semiconductor Spintronics. *Nat. Phys.* **2007**, *3* (3), 153−159.

(6) Picozzi, S. Ferroelectric Rashba Semiconductors as A Novel Class of Multifunctional Materials. *Frontiers in Physics* **2014**, *2* (10), 1−5.

(7) Narayan, A. Class of Rashba Ferroelectrics in Hexagonal Semiconductors. *Phys. Rev. B* **2015**, *92* (22), 220101.

(8) Chen, J.; Wu, K.; Hu, W.; Yang, J. High-throughput Inverse Design for 2D Ferroelectric Rashba Semiconductors. *J. Am. Chem. Soc.* **2022**, *144* (43), 20035−20046.

(9) Zhou, B. Ferroelectric Rashba Semiconductors, $AgBiP_2X_6$ (X = S, Se And Te), with Valley Polarization: an Avenue Towards Electric and Nonvolatile Control of Spintronic Devices. *Nanoscale* **2020**, *12* (9), 5533−5542.

(10) Bruyer, E.; Di Sante, D.; Barone, P.; Stroppa, A.; Whangbo, M.-H.; Picozzi, S. Possibility of Combining Ferroelectricity and Rashba-like Spin Splitting in Monolayers of The 1T-type Transition Metal Dichalcogenides MX_2(M = Mo,W; X = S, Se, Te). *Phys. Rev. B* **2016**, *94* (19), 195402.

(11) Lin, Z.; Si, C.; Duan, S.; Wang, C.; Duan, W. Rashba Splitting in Bilayer Transition Metal Dichalcogenides Controlled by Electronic Ferroelectricity. *Phys. Rev. B* **2019**, *100* (15), 155408.
(12) Varotto, S.; Nessi, L.; Cecchi, S.; Sławińska, J.; Noël, P.; Petrò, S.; Fagiani, F.; Novati, A.; Cantoni, M.; Petti, D.; et al. Room-temperature Ferroelectric Switching of Spin-to-charge Conversion in Germanium Telluride. *Nat. Electron.* **2021**, *4* (10), 740−747.
(13) Li, J.; Yang, X.; Liu, Y.; Huang, B.; Wu, R.; Zhang, Z.; Zhao, B.; Ma, H.; Dang, W.; Wei, Z.; et al. General Synthesis of Two-dimensional van der Waals Heterostructure Arrays. *Nature* **2020**, *579* (7799), 368−374.
(14) Liu, Y.; Weiss, N. O.; Duan, X.; Cheng, H.-C.; Huang, Y.; Duan, X. Van der Waals Heterostructures and Devices. *Nat. Rev. Mater.* **2016**, *1* (9), 16042.
(15) Ji, J.; Song, X.; Liu, J.; Yan, Z.; Huo, C.; Zhang, S.; Su, M.; Liao, L.; Wang, W.; Ni, Z.; et al. Two-dimensional Antimonene Single Crystals Grown by van der Waals Epitaxy. *Nat. Commun.* **2016**, *7* (1), 13352.
(16) Ding, W.; Zhu, J.; Wang, Z.; Gao, Y.; Xiao, D.; Gu, Y.; Zhang, Z.; Zhu, W. Prediction of Intrinsic Two-dimensional Ferroelectrics in In_2Se_3 and Other III2-VI3 van der Waals Materials. *Nat. Commun.* **2017**, *8* (1), 14956.
(17) Zhou, Y.; Wu, D.; Zhu, Y.; Cho, Y.; He, Q.; Yang, X.; Herrera, K.; Chu, Z.; Han, Y.; Downer, M. C.; et al. Out-of-plane Piezoelectricity and Ferroelectricity in Layered α-In_2Se_3 Nanoflakes. *Nano Lett.* **2017**, *17* (9), 5508−5513.
(18) Gong, C.; Kim, E. M.; Wang, Y.; Lee, G.; Zhang, X. Multiferroicity in Atomic van der Waals Heterostructures. *Nat. Commun.* **2019**, *10* (1), 2657.
(19) Cheng, H.-X.; Zhou, J.; Wang, C.; Ji, W.; Zhang, Y.-N. Nonvolatile Electric Field Control of Magnetism in Bilayer CrI_3 on Monolayer In_2Se_3. *Phys. Rev. B* **2021**, *104* (6), 064443.
(20) Eom, J.; Lee, I. H.; Kee, J. Y.; Cho, M.; Seo, J.; Suh, H.; Choi, H.-J.; Sim, Y.; Chen, S.; Chang, H. J.; et al. Voltage Control of Magnetism In $Fe_{3-X}GeTe_2/In_2Se_3$ van der Waals Ferromagnetic/Ferroelectric Heterostructures. *Nat. Commun.* **2023**, *14* (1), 5605.
(21) Shi, Z.-Q.; Li, H.; Yuan, Q.-Q.; Song, Y.-H.; Lv, Y.-Y.; Shi, W.; Jia, Z.-Y.; Gao, L.; Chen, Y.-B.; Zhu, W.; Li, S.-C. Van der Waals Heteroepitaxial Growth of Monolayer Sb in a Puckered Honeycomb Structure. *Adv. Mater.* **2019**, *31* (5), 1806130.
(22) Kresse, G.; Joubert, D. From Ultrasoft Pseudopotentials to The Projector Augmented-wave Method. *Phys. Rev. B* **1999**, *59* (3), 1758−1775.
(23) Blöchl, P. E. Projector augmented-wave Method. *Phys. Rev. B* **1994**, *50* (24), 17953−17979.
(24) Kresse, G.; Furthmüller, J. Efficient Iterative Schemes for ab initio Total-energy Calculations using a Plane-Wave Basis Set. *Phys. Rev. B* **1996**, *54* (16), 11169−11186.
(25) Kresse, G.; Furthmüller, J. Efficiency of ab-initio Total Energy Calculations for Metals and Semiconductors using a Plane-wave Basis Set. *Comput. Mater. Sci.* **1996**, *6* (1), 15−50.
(26) Perdew, J. P.; Burke, K.; Ernzerhof, M. Perdew, Burke, and Ernzerhof Reply. *Phys. Rev. Lett.* **1998**, *80* (4), 891−891.
(27) Perdew, J. P.; Burke, K.; Ernzerhof, M. Generalized Gradient Approximation Made Simple. *Phys. Rev. Lett.* **1996**, *77* (18), 3865−3868.
(28) Klimeš, J.; Bowler, D. R.; Michaelides, A. Chemical Accuracy for the van der Waals Density Functional. *J. Phys.: Condens. Matter* **2010**, *22* (2), 022201.
(29) Dion, M.; Rydberg, H.; Schröder, E.; Langreth, D. C.; Lundqvist, B. I. Van der Waals Density Functional for General Geometries. *Phys. Rev. Lett.* **2004**, *92* (24), 246401.
(30) Klimeš, J.; Bowler, D. R.; Michaelides, A. Van der Waals Density Functionals Applied to Solids. *Phys. Rev. B* **2011**, *83* (19), 195131.
(31) Steiner, S.; Khmelevskyi, S.; Marsmann, M.; Kresse, G. Calculation of the Magnetic Anisotropy with Projected-augmented-wave Methodology and The Case Study of Disordered $Fe_{1-X}Co_x$ Alloys. *Phys. Rev. B* **2016**, *93* (22), 224425.
(32) Herath, U.; Tavadze, P.; He, X.; Bousquet, E.; Singh, S.; Muñoz, F.; Romero, A. H. Pyprocar: a Python Library for Electronic Structure Pre/Post-processing. *Comput. Phys. Commun.* **2020**, *251*, 107080.
(33) Henkelman, G.; Uberuaga, B. P.; Jónsson, H. A Climbing Image Nudged Elastic Band Method for Finding Saddle Points and Minimum Energy Paths. *J. Chem. Phys.* **2000**, *113* (22), 9901−9904.
(34) Chuang, F.-C.; Hsu, C.-H.; Chen, C.-Y.; Huang, Z.-Q.; Ozolins, V.; Lin, H.; Bansil, A. Tunable Topological Electronic Structures in Sb(111) Bilayers: a First-principles Study. *Appl. Phys. Lett.* **2013**, *102* (2), 022424.
(35) Bucher, D.; Pierce, L. C. T.; McCammon, J. A.; Markwick, P. R. L. On the Use of Accelerated Molecular Dynamics to Enhance Configurational Sampling in ab initio Simulations. *J. Chem. Theory Comput.* **2011**, *7* (4), 890−897.
(36) Togo, A.; Tanaka, I. First Principles Phonon Calculations in Materials Science. *Scripta Materialia* **2015**, *108*, 1−5.
(37) Jiang, S.; Nazir, S.; Yang, K. Origin of the Large Interfacial Perpendicular Magnetic Anisotropy In MgO/Co_2FeAl. *Phys. Rev. B* **2020**, *101* (13), 134405.
(38) Behtash, M.; Wong, J.; Jiang, S.; Luo, J.; Yang, K. First-Principles Study of Impurity Segregation in Zirconia, Hafnia, and Yttria-stabilized-zirconia Grain Boundaries. *J. Eur. Ceram. Soc.* **2019**, *39* (13), 3812−3820.
(39) Manchon, A.; Koo, H. C.; Nitta, J.; Frolov, S. M.; Duine, R. A. New Perspectives for Rashba Spin-orbit Coupling. *Nat. Mater.* **2015**, *14* (9), 871−882.
(40) Tang, X.; Shang, J.; Ma, Y.; Gu, Y.; Chen, C.; Kou, L. Tuning Magnetism of Metal Porphyrazine Molecules by a Ferroelectric In_2Se_3 Monolayer. *ACS Appl. Mater. Interfaces* **2020**, *12* (35), 39561−39566.
(41) Tang, X.; Shang, J.; Gu, Y.; Du, A.; Kou, L. Reversible Gas Capture using a Ferroelectric Switch and 2D Molecule Multiferroics on the In_2Se_3 Monolayer. *J. Mater. Chem. A* **2020**, *8* (15), 7331−7338.
(42) Kwon, K. C.; Zhang, Y.; Wang, L.; Yu, W.; Wang, X.; Park, I.-H.; Choi, H. S.; Ma, T.; Zhu, Z.; Tian, B.; et al. In-plane Ferroelectric Tin Monosulfide and Its Application in a Ferroelectric Analog Synaptic Device. *ACS Nano* **2020**, *14* (6), 7628−7638.
(43) Xiang, L.; Ke, Y.; Zhang, Q. Tunable Giant Rashba-type Spin Splitting in $PtSe_2/MoSe_2$ Heterostructure. *Appl. Phys. Lett.* **2019**, *115* (20), 203501.

https://doi.org/10.1021/acsami.4c07562
ACS Appl. Mater. Interfaces XXXX, XXX, XXX−XXX